A new non-eddy viscosity subgrid-scale model and its application to channel flow

By K. B. Shah AND J. H. Ferziger

1. Motivation and objectives

To date, most large-eddy simulations (LES) have been carried out with eddy viscosity subgrid scale (SGS) models, with only a few exceptions that used the mixed model. Even though the assumptions behind Smagorinsky's model are rather stringent, it has been applied successfully to a variety of turbulent flows. This success is attributed to the ability of eddy viscosity models to drain energy from large scales, thus simulating the dissipative nature of turbulence. Most SGS models are absolutely dissipative i.e. they remove energy from the large scales at every instant. However, SGS stresses may transfer energy back to the large scales intermittently; this reverse transfer or backscatter is especially important in geophysical flows and in transition. In a fully developed channel flow, there is reverse flow of energy from small to large scales near the walls (Härtel & Kleiser 1993), but eddy viscosity models are unable to account for this important feature. The dynamic localization eddy viscosity model of Ghosal *et al.* (1995) allows backscatter by co-evolving an auxiliary equation for the SGS energy; however, the computational cost is considerably larger than for conventional SGS models (Cabot 1994). In this report, a new non-eddy viscosity model based on local approximation of total quantities in terms of filtered ones is introduced; the scale similarity model of Bardina (1983) is a special case of this model. This procedure does not require the assumption of homogeneity, permits backscatter of energy from small to large scales, and is readily implemented in finite difference codes.

The results of applying the proposed model to second order finite volume simulation of plane channel flow at high Reynolds numbers ($Re_b = 38000$) is described in this report. Greater emphasis is placed on the high Reynolds number flow since it provides a more rigorous test of the SGS model and its potential application. The results are compared to ones produced by the conventional and dynamic Smagorinsky models and the spectral LES of Piomelli (1993).

2. Accomplishments

2.1 Numerical method

A second order staggered finite volume formulation is used to discretize the Navier-Stokes equations. Uniform meshes are used in the streamwise and the spanwise directions, and hyperbolic tangent stretching is used in the wall-normal direction. A fractional step method is used to decouple the pressure from the momentum equation. The momentum equations are first advanced without satisfying continuity, then the velocity field is adjusted to satisfy continuity. The time advancement

of the momentum equation is semi-implicit, explicit third order Runge-Kutta for the non-linear (convective) terms and implicit second order Crank-Nicolson for the diffusive (viscous) terms. Continuity is enforced by solving a Poisson equation for a pressure-like variable; a fast Fourier transform (FFT) procedure solves this problem efficiently. A full description of this numerical method can be found in Yang *et al.* (1993)

2.2 Computational domain and boundary conditions

The computational domain parameters are listed in table (1). The x, y, and z axes are along the streamwise, wall-normal, and spanwise directions, respectively. The simulations were carried out by fixing the mass flow (or Re_b) rather than the pressure gradient (or skin friction). The physical domain size and grid size are similar to that of Piomelli (1993); however, since Re_τ in present simulation (≈ 1800) is slightly lower than Piomelli's value ($Re_\tau = 1995$), the domain and grid sizes in wall units are slightly different. Reynolds numbers are based on the half channel height δ, bulk velocity U_b for Re_b, and the friction velocity u_τ for Re_τ.

Re_b	Re_τ	(Nx, Ny, Nz)	(Lx, Ly, Lz)	$(\Delta x^+, \Delta z^+)$	$(\Delta y^+_{min}, \Delta y^+_{max})$
38000	≈ 1800	$(64, 80, 80)$	$(2.5\pi, 2.0, 0.5\pi)$	$\approx (221, 35)$	$\approx (1.5, 150)$

TABLE 1: Simulation parameters

2.3 The proposed model

In LES, the effect of unresolved scales of motions on large scales appears through the SGS stress:

$$\tau_{ij} = \overline{u_i u_j} - \overline{u}_i\, \overline{u}_j \tag{1}$$

which must be modeled. Most SGS models employ eddy viscosities, which assume a linear relationship between the anisotropic part of SGS stress tensor and the large scale strain rate tensor. The isotropic part is absorbed into the large scale pressure field. Thus

$$\tau^a_{ij} = \tau_{ij} - \frac{\delta_{ij}}{3}\tau_{ii} = -2\nu_t \overline{S}_{ij} = -\nu_t \left(\frac{\partial \overline{u}_i}{\partial x_j} + \frac{\partial \overline{u}_j}{\partial x_i} \right)$$

The eddy viscosity ν_t is usually taken to be:

$$\nu_t = (C_s \Delta)^2 |\overline{S}|$$

where Δ is the length scale of a typical SGS eddy and C_s is the model parameter which depends on the flow. The dynamic model proposed by Germano *et al.* (1991) computes this parameter in tandem with the calculation. This procedure has been used with remarkable success for a variety of flows, but the model coefficient has large fluctuations with positive and negative values nearly as likely (Lund *et al.* 1993). Numerical instability due to large negative viscosity can be eliminated by averaging in homogeneous directions (Lilly 1992), but this is not very satisfactory.

Recently, a dynamic localization model (Ghosal *et al.* 1995) has been developed which permits negative eddy viscosities by limiting the time that eddy viscosities remain negative by co-evolving the SGS kinetic energy. The equation for SGS energy contains additional model coefficients. The advantage of this method remains to be established in light of its complexity and additional cost.

The scale similarity model of Bardina (1983), a non-eddy viscosity model, is appealing in this respect. It permits backscatter and provides a good representation of instantaneous energy transfer between the large and small scales; however, it fails to provide enough mean dissipation. The scale similarity model can be easily derived by substituting $u_i \approx \overline{u}_i$ in the expression for the exact SGS stress $\tau_{ij} = \overline{u_i\, u_j} - \overline{u}_i\, \overline{u}_j$ which yields a Galilean invariant version of this model:

$$\tau_{ij} = \overline{\overline{u}_i\, \overline{u}_j} - \overline{\overline{u}}_i\, \overline{\overline{u}}_j$$

The mean dissipation is small because forward and backward transfer of energy are nearly balanced. It is plausible that if higher order terms are included in the approximation for u_i instead of $u_i \approx \overline{u}_i$, this model might provide sufficient mean dissipation yet retain the favorable characteristics. Thus, the following form for the SGS stress is proposed:

$$\tau_{ij} = \widehat{u_i^\star\, u_j^\star} - \widehat{u_i^\star}\, \widehat{u_j^\star} \tag{2}$$

where $u_i^\star$ is defined implicitly in terms of the filtered velocity $\overline{u}_i$:

$$\mathcal{L}(u_i^\star) = \overline{u}_i \qquad \mathcal{L} = \mathcal{L}_x \mathcal{L}_y \mathcal{L}_z$$

where $\mathcal{L}_x$ is of the form:

$$\mathcal{L}_x = \left(1 + C_1^\star(\Delta_x)\frac{\partial}{\partial x} + C_2^\star(\Delta_x)\frac{\partial^2}{\partial x^2}\right)$$

$\mathcal{L}_y$ and $\mathcal{L}_z$ are of the similar form. The $\widehat{\ }$ operation is also defined in a similar manner:

$$\widehat{u_i^\star} = \mathcal{V}(u_i^\star) \qquad \mathcal{V} = \mathcal{V}_x \mathcal{V}_y \mathcal{V}_z$$

where $\mathcal{V}$ is similar to the $\mathcal{L}$ operator:

$$\mathcal{V}_x = \left(1 + \widehat{C_1}(\Delta_x)\frac{\partial}{\partial x} + \widehat{C_2}(\Delta_x)\frac{\partial^2}{\partial x^2}\right)$$

$C_1^\star, C_2^\star, \widehat{C_1}$, and $\widehat{C_2}$ are given functions of the local filter width Δ.

This approximation is an extension of the filtering operation. To understand this procedure, consider the expression for $u_i^\star$ in one dimension:

$$\overline{u}_i \approx u_i^\star + C_1^\star(\Delta)\, \frac{du_i^\star}{dx} + C_2^\star(\Delta)\, \frac{d^2 u_i^\star}{dx^2} \tag{3}$$

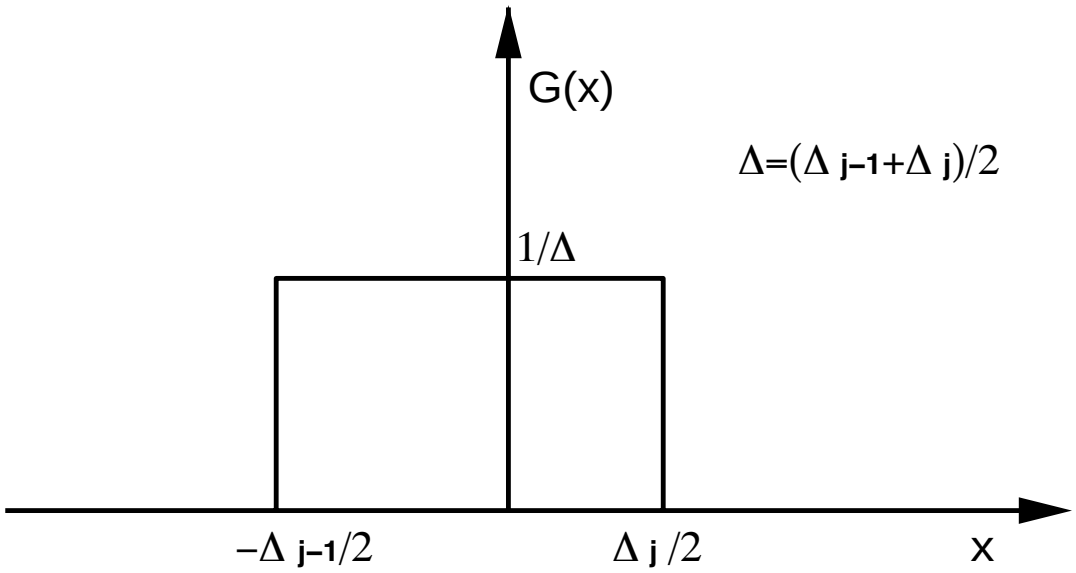

FIGURE 1. A non-symmetrical Box filter.

This is a local Taylor series approximation of the filtered quantity in terms of the unfiltered quantity. For the non-symmetrical box filter defined by Fig. 1:

$$G_j = G(x - x_j) = \begin{cases} 1/\Delta, & \text{if} \quad -\Delta_{j-1}/2 < x - x_j < \Delta_j/2; \\ 1/(2\Delta), & \text{if} \quad x - x_j = -\Delta_{j-1}/2 \text{ or } x - x_j = \Delta_j/2; \\ 0, & \text{if} \quad x - x_j < -\Delta_{j-1}/2 \text{ or } x - x_j > \Delta_j/2. \end{cases}$$

where $\Delta = (\Delta_j + \Delta_{j-1})/2$ is the filter width, the filtering operation defined by:

$$\overline{u(x)} = \int_{-\infty}^{\infty} G(x - x')\ u(x')\ dx'$$

reduces to:

$$\overline{u(x_j)}^{\Delta} = \frac{2}{(\Delta_j + \Delta_{j-1})} \int_{x_j - \frac{\Delta_{j-1}}{2}}^{x_j + \frac{\Delta_j}{2}} u(x')\ dx'$$

Taylor series expansion of $u(x')$ around x_j leads to

$$\overline{u(x_j)}^{\Delta} = u(x_j) + \frac{(\Delta_j - \Delta_{j-1})}{4} u'(x_j) + \frac{(\Delta_j^2 - \Delta_j \Delta_{j-1} + \Delta_{j-1}^2)}{24} u''(x_j) + O(\Delta^3) \quad (4)$$

Equation (3) is a second order approximation to Eq. (4). Extension to three dimensions consists of sequential application of $\mathcal{L}$ operators in each direction, but $u^\star$ is no longer a second order approximation u. The coefficients are functions of the local filter widths, which depend on the choice of the filter-grid ratio (FGR) i.e.

the ratio of local filter width Δ to the mesh size. A finite difference approximation to Eq. (3) is:

$$\overline{u_i} = a\ u^\star_{i-1} + b\ u^\star_i + c\ u^\star_{i+1} \tag{5}$$

where a, b, and c can be expressed in terms of the filter width Δ and the grid size h. For filter width equal to the local mesh size $\Delta = (h_j + h_{j-1})/2$, the coefficients a, b, and c can be expressed using the Taylor series:

$$\begin{aligned} a &= \frac{h_{j-1}^2 + 2h_{j-1}h_j - 2h_j^2}{12h_{j-1}(h_{j-1} + h_j)} \\ c &= \frac{h_j^2 + 2h_{j-1}h_j - 2h_{j-1}^2}{12h_j(h_{j-1} + h_j)} \\ b &= 1 - (a + c) \end{aligned} \tag{6}$$

where $h_j = x_{j+1} - x_j$. The extension to three dimensions involves sequential application of Eq. (5) in each direction. The solution procedure requires inversion of tridiagonal systems. Details of the implementation of this model are presented in Shah (1996).

Even though the forms of $\mathcal{L}$ and $\mathcal{V}$ are the same, it is not necessary to use the same coefficients in the $\mathcal{L}$ and $\mathcal{V}$ operators. Bardina's scale similarity model is a special case of this model; for $\mathcal{L} = 1$ and the $\widehat{\ }$ filter corresponding to the grid filter. Bardina's model may be viewed as a zeroth order approximation ($u_i \approx \overline{u}_i$) of the total quantity. Strictly speaking, it is not a model because it is the Leonard term of the Galilean invariant decomposition of the exact SGS stress (Germano, 1986). The proposed model uses a higher order approximation of the total quantity, and the Leonard term is automatically incorporated. The SGS stress is constructed from the field $u_i^\star$ which is obtained from the filtered field $\overline{u}_i$ by approximating the high wavenumber spectrum in a prescribed manner (as in Eq. (3)) dependent on the choice of filter-grid ratio.

Even though Taylor series expansion cannot be used for Fourier cutoff filters, the model equations (for $\mathcal{L}$ and $\mathcal{V}$) are still valid. The fundamental idea is to construct the SGS stress from the filtered velocity field. The high wavenumber region is expected to be representative of the SGS as most of the interaction between the resolved field and the SGS field take place at these scales. Finally, it must be pointed out that the coefficients $C_1^\star$ and $C_2^\star$ need not be the same as the coefficients in the one dimensional expansion Eq. (4). Two major approximations have been made to the filtering operation; the cross derivative terms that arise in three dimensions and the higher order terms are ignored. The effect of these terms are accounted for by the two coefficients $C_1^\star$ and $C_2^\star$. However, in the present work, we have taken them to be what one gets from a truncated expansion of the box filtering in one dimension (Eq. (4)).

This procedure does not require an assumption of homogeneity. Since it is not an eddy viscosity model, it does not suffer from instability due to negative eddy viscosity. Backscatter of energy from small to large scales, if it exists, is a natural part of the simulation. This procedure has the added advantage of providing an

estimate of the total turbulence quantities. For high Reynolds numbers at which the SGS energy may be significant, this can lead to improved comparisons with physical quantities.

2.4 Results for high Reynolds number ($Re_b = 38000$) plane channel flow

Results from high Re simulations are compared to the spectral LES of Piomelli (1993), which is in good agreement with experimental results. Several simulations were carried out to assess the accuracy of the SGS model and the effect of parameters such as the type of filter employed in the dynamic model and filter-grid ratios (FGR) in the new model. First, we present comparison of mean and turbulent quantities for four cases: no model (CDNS1), Smagorinsky's model with Van Driest (1956) wall damping (SMAG1), dynamic Smagorinsky model with filtering in the homogeneous directions (DSMAG1), and the proposed model with filter-grid ratio = 2.0 (NEWM3). Other results will be presented later to show the effect of filters on the dynamic model and the effect of filter-grid ratio on the new model.

The profile of the mean velocity normalized by skin friction velocity (u_τ) is shown in Figs. 2 & 3 along with Piomelli's spectral LES data and the log law $U^+ = (1/\kappa)\log y^+ + A$ with $\kappa = 0.4$ and $A = 5.5$. The profiles obtained from current LES are characterized by a bulge in the region $10 < y^+ < 200$, and the slope in the log law region is smaller than $1/\kappa = 2.5$. The coarse grid DNS shows a smaller bulge, but there is no improvement in the slope of the profile. The mean velocity profile for the new model is in better agreement with Piomelli's LES and the log law, but the bulge is still present. Interestingly, the new model profile falls below the log law for $300 < y^+ < 800$, in contrast to other models including the coarse DNS which over-predicts the mean velocity through out the channel. Both coarse DNS and the new model fall on the log law and Piomelli's LES for $y^+ > 1000$. Table (2) show a comparison of the skin friction coefficient $c_f = \tau_w/\frac{1}{2}\rho U_b^2$ and the ratio of centerline velocity (U_c) to the bulk velocity (U_b) with the experimental correlations proposed by Dean (1978):

	Re_b	$\frac{c_f - c_f^{Dean}}{c_f^{Dean}} \times 100$	U_c/U_b
Dean (1978)	38000		1.124
Smagorinsky (SMAG1)	38000	-5.77	1.086
Dynamic Smag. (DSMAG1)	38000	-8.31	1.090
New Model (DNEWM3)	38000	+2.30	1.110
No model (CDNS1)	38000	+0.25	1.094
Piomelli	42598	+1.75	1.105

TABLE 2: Comparison of the skin friction and centerline velocity with experimental correlations of Dean (1978)

Both the skin friction and the centerline velocity predicted by the new model and the coarse DNS are within 2.5% of Dean's correlation. The conventional Smagorinsky and the dynamic model under-predict the skin friction, which causes the mean velocity profile to rise above the log law.

The rms of *filtered* streamwise velocity normalized by the skin friction velocity is shown in Fig. 4 along with Piomelli's result. The effect of SGS models is now quite pronounced. The Smagorinsky, dynamic, and coarse DNS over-predict the peak in streamwise fluctuations by 40%, but the new model results compare well with Piomelli's. Fig. 5 shows the streamwise fluctuations in global units. All the models under-predict it far from the wall. The SGS contribution, which can be significant, has not been added, but this addition will worsen the results near the wall, which are already too high. Figs. 6, 7, 8, and 9 show the spanwise and wall-normal fluctuations in wall and global units. The predictions of the new model lie below those of other models. Since the streamwise energy is redistributed to the other two components via the pressure-strain interaction, which acts as a sink for the streamwise component and as a source for the spanwise and wall-normal components, larger streamwise fluctuations lead to larger fluctuations in the other two directions.

Figure 10 shows the SGS shear stress τ_{12}^{SGS} for various models; clearly the new model produces the largest SGS stress by far. The SGS stress accounts for 28% of the total stress ($\overline{u}\,\overline{v}+\tau_{12}^{SGS}$) in the new model as opposed to 2% for the Smagorinsky and dynamic models. Far from the walls, the new model produces a significant SGS contribution. It is desirable to compare the total fluctuations (resolved+SGS); however, for Smagorinsky models it is difficult to compute the SGS contribution. Bardina (1983) proposed the following expression for the total turbulent intensity $Q^2 =< u_i\, u_i >$ from the turbulent intensity of the filtered field $Q_f^2 =< \overline{u}_i\, \overline{u}_i >$ and the SGS dissipation rate ϵ:

$$Q^2 = \frac{Q_f^4}{Q_f^2 - c(2\Delta_f \epsilon_f)^{2/3}}$$

where Δ_f is the filter width and $c = 1.04$. Bardina used this estimate to determine the total kinetic energy in various types of homogeneous turbulence and found good agreement with experiments. Figs. 11 & 12 show the total turbulent kinetic energy $Q^2/2$ for the various models. Bardina's estimate was applied to all models except the new model, which evaluates the SGS contribution directly. From Fig. 11 it is evident that SGS models do poorly near the walls. Figs. 11 & 12 show Piomelli's *filtered* fluctuation since it is in good agreement with the experiments, but it too will deteriorate near the wall if the SGS contribution is included. All models except the new model over-predict the peak by almost 70%; the new model does better but over-predicts it by 20%. Table (3) shows the fraction of total turbulent kinetic energy η in the subgrid scales:

$$\eta = \frac{\int_0^{2\delta}(Q^2 - Q_f^2)dy}{\int_0^{2\delta} Q^2\, dy}$$

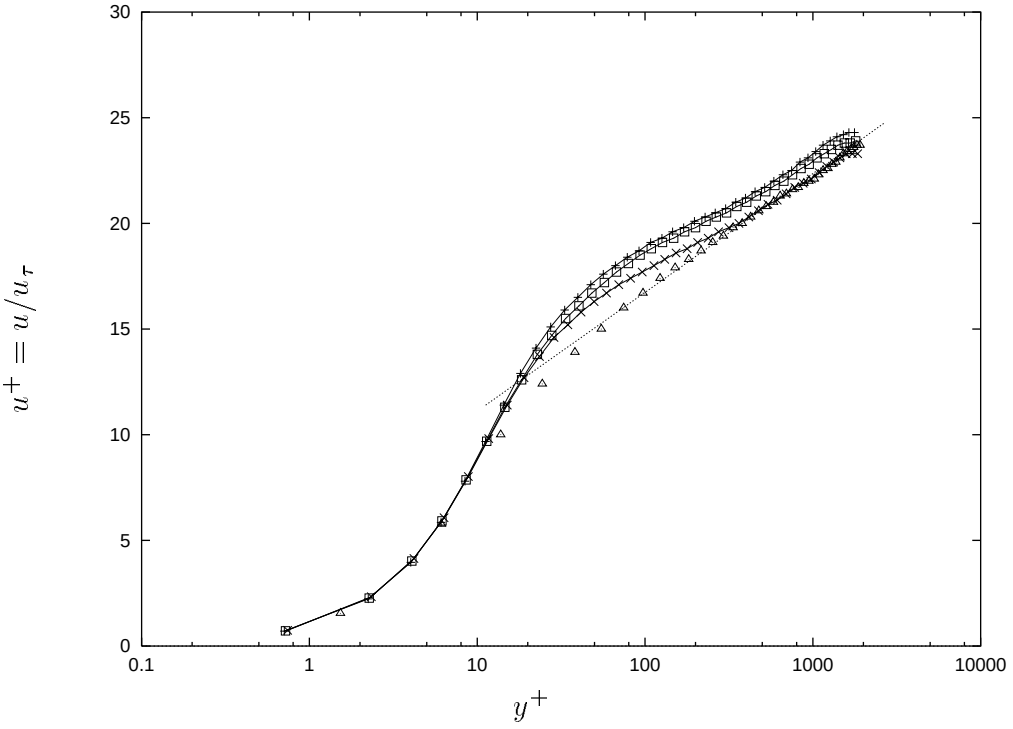

FIGURE 2. Mean velocity profiles at $Re_b = 38000$. ····· log law; —□— Smagorinsky (SMAG1); – + – dynamic (DSMAG1); —×— no model (CDNS1); △ spectral LES of Piomelli (1993).

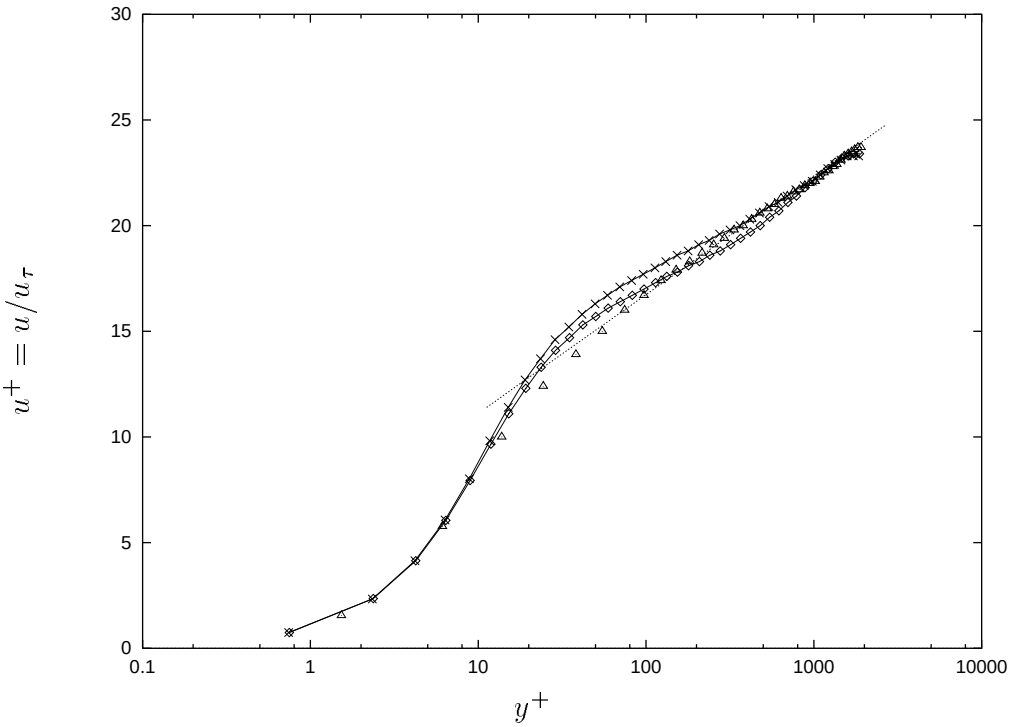

FIGURE 3. Mean velocity profiles at $Re_b = 38000$. ····· log law; —×— no model (CDNS1); —◇— proposed model; △ spectral LES of Piomelli (1993).

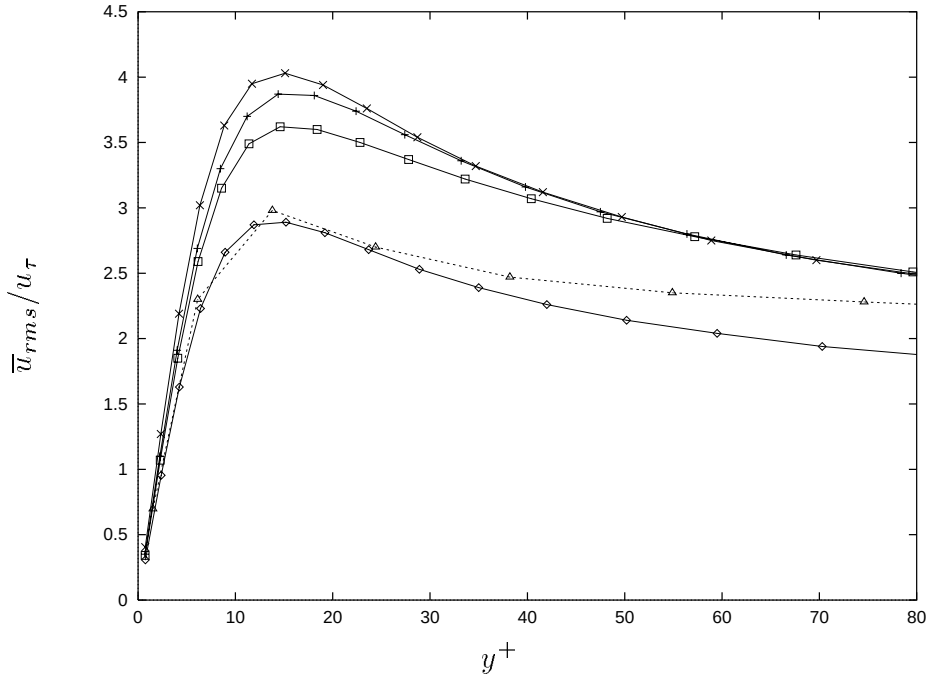

FIGURE 4. RMS of the *resolved* streamwise velocity at $Re_b = 38000$ in wall units. —□— Smagorinsky (SMAG1); –+– dynamic (DSMAG1); —×— no model (CDNS1); —◇— proposed model (NEWM3); △ spectral LES of Piomelli (1993).

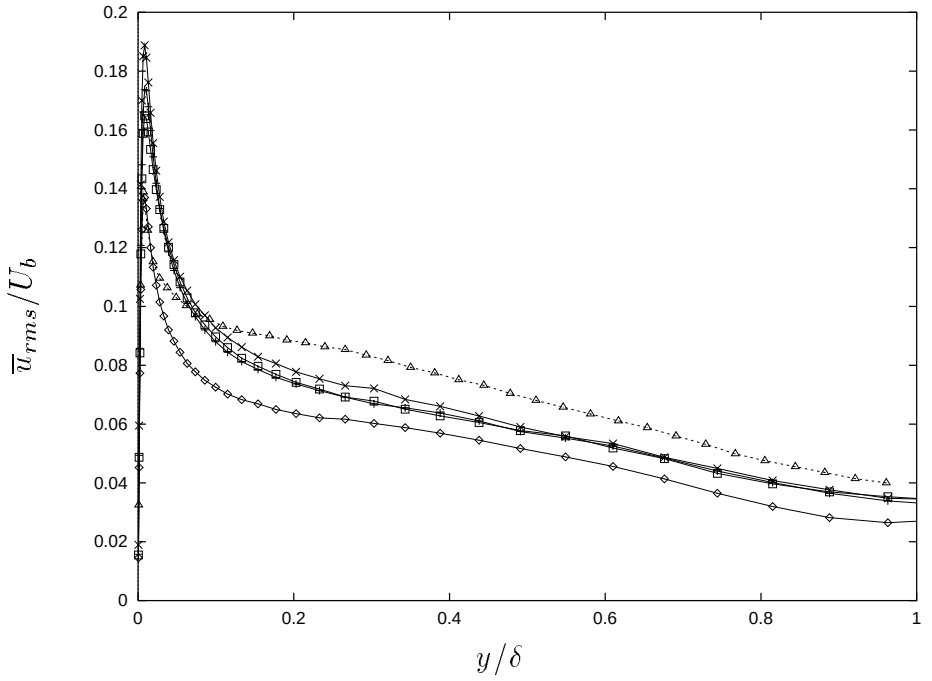

FIGURE 5. RMS of the *resolved* streamwise velocity at $Re_b = 38000$ in global units. —□— Smagorinsky (SMAG1); –+– dynamic (DSMAG1); —×— no model (CDNS1); —◇— proposed model (NEWM3); △ spectral LES of Piomelli (1993).

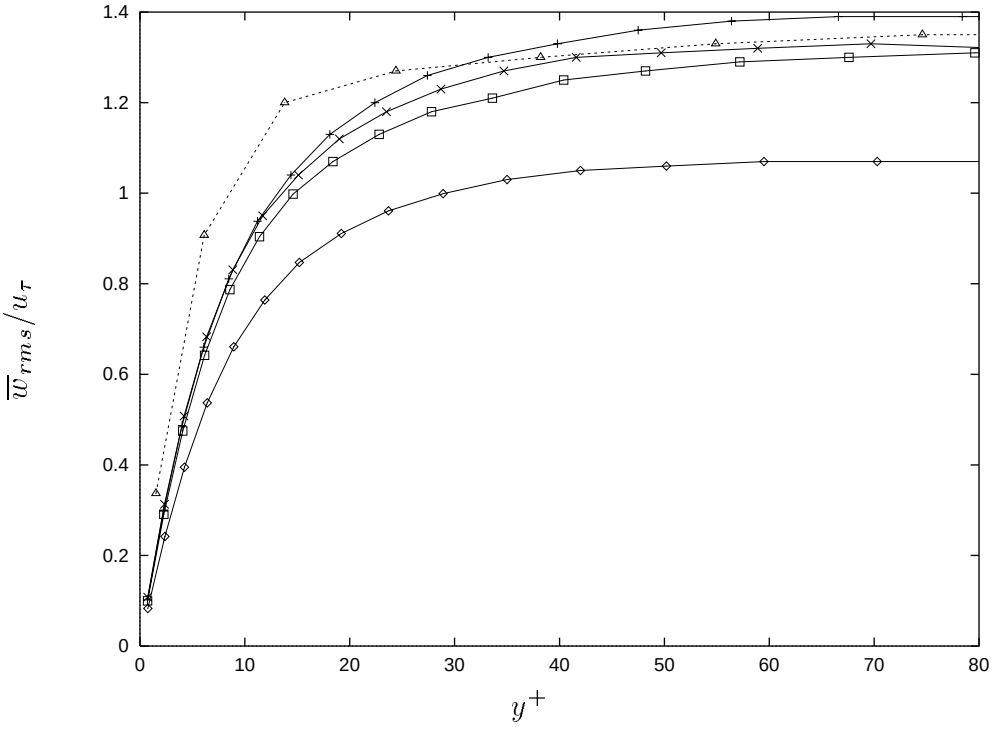

FIGURE 6. RMS of *resolved* spanwise velocity at $Re_b = 38000$ in wall units. —□— Smagorinsky (SMAG1); – + – dynamic (DSMAG1); —×— no model (CDNS1); —◇— proposed model (NEWM3); △ spectral LES of Piomelli (1993).

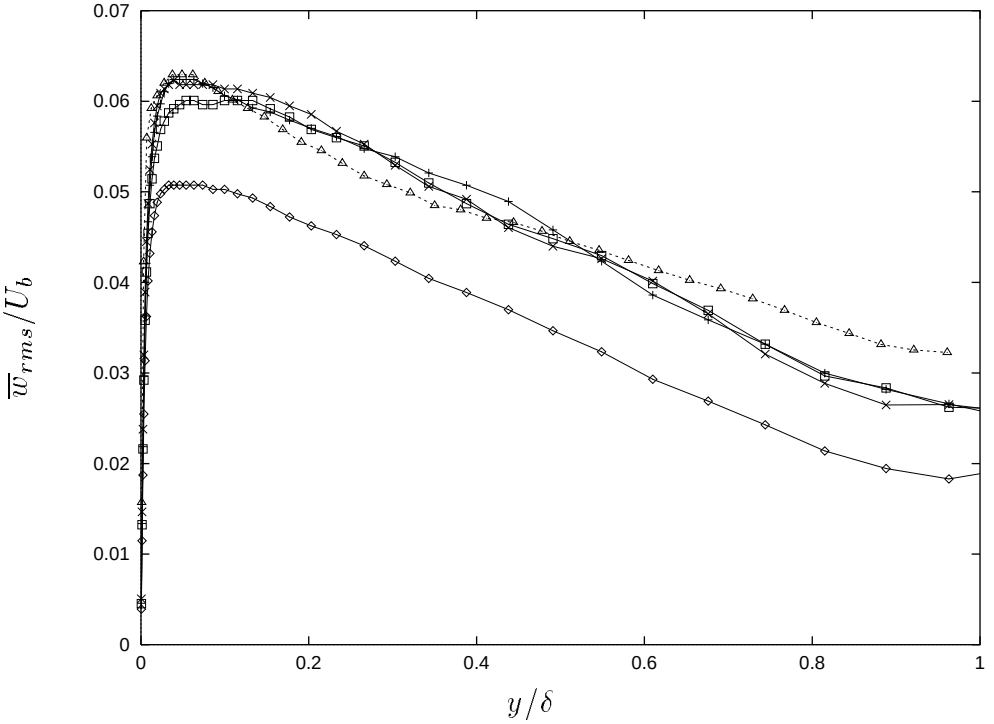

FIGURE 7. RMS of the *resolved* spanwise velocity at $Re_b = 38000$ in global units. —□— Smagorinsky (SMAG1); – + – dynamic (DSMAG1); —×— no model (CDNS1); —◇— proposed model (NEWM3); △ spectral LES of Piomelli (1993).

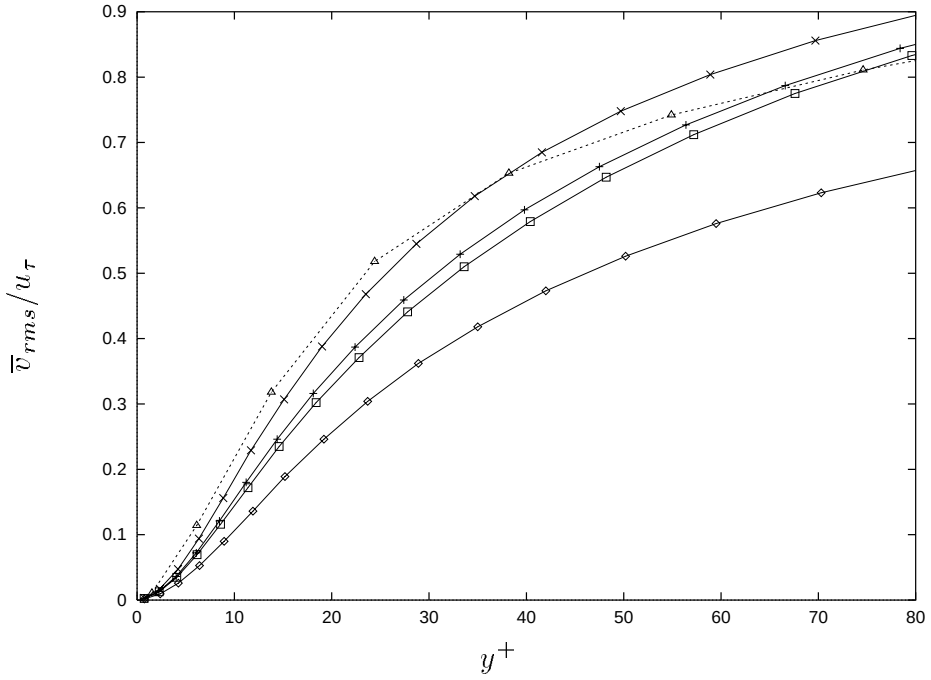

FIGURE 8. RMS of the *resolved* wall-normal velocity at $Re_b = 38000$ in wall units. —□— Smagorinsky (SMAG1); –+– dynamic (DSMAG1); —×— no model (CDNS1); —◇— proposed model (NEWM3); △ spectral LES of Piomelli (1993).

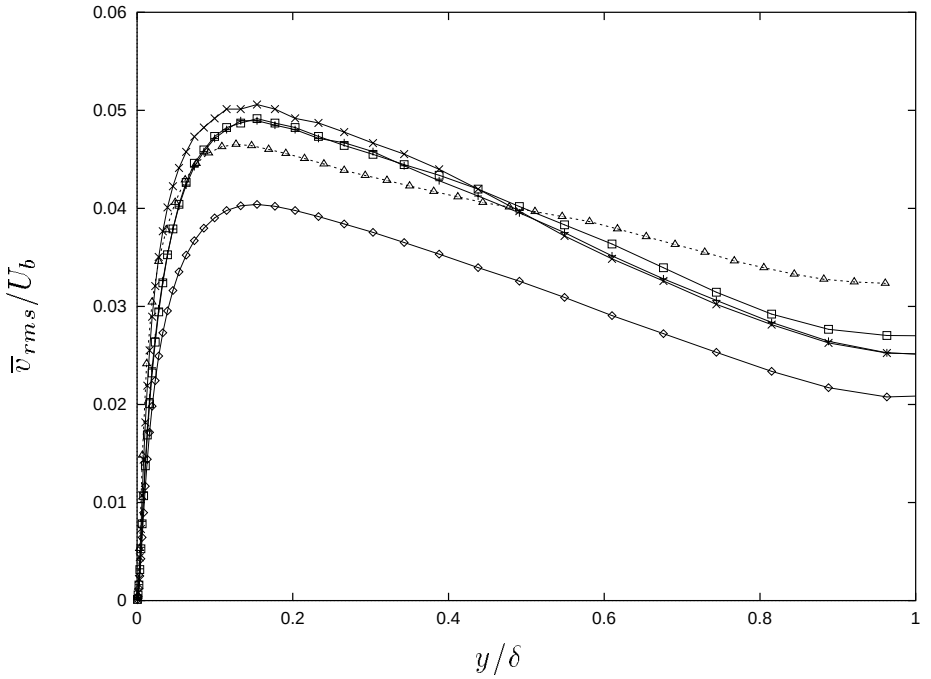

FIGURE 9. RMS of the *resolved* wall-normal velocity at $Re_b = 38000$ in global units. —□— Smagorinsky (SMAG1); –+– dynamic (DSMAG1); —×— no model (CDNS1); —◇— proposed model (NEWM3); △ spectral LES of Piomelli (1993).

A significant portion of the energy resides in SGS in the proposed model (44%). The new model extracts considerable energy from the large scales, creating energetic subgrid scales. But in the Smagorinsky and dynamic models, the energy piles up in the large scales because the SGS stress is unable to drain enough energy from the large scales. As a result, the skin friction is under-predicted since the dissipation and skin friction are directly related.

	η
Smagorinsky (SMAG1)	0.08
Dynamic Smag. (DSMAG1)	0.07
New Model (DNEWM3)	0.44

TABLE 3: Fraction of turbulent kinetic energy in the subgrid scales.

Figure 13 shows the mean SGS dissipation rate $< \epsilon_{SGS} > = < \tau_{ij}\overline{S}_{ij} >$ near the wall for various models. The dissipation rate is normalized by U_b instead of u_τ, which is different for each model. The dynamic model has the smallest peak and the smallest overall SGS dissipation rate. For fully developed channel flow the total dissipation rate (viscous+SGS) is proportional to the pressure drop. Since the dynamic model has the lowest skin friction, the total dissipation is also the smallest. Also, the total dissipation rate from the Smagorinsky and dynamic models are smaller than the coarse DNS (since skin friction is smaller), but the total dissipation rate of the new model is larger. Figures 14 & 15 show the time series of dissipation rate at $x = 1.25\pi$, $z = 0.25\pi$ and $y^+ = 2$, and 12. Significant backscatter of energy is seen in the buffer region and beyond. In the region close to the wall, $y^+ = 2$, the dissipation rate is mostly negative. Away from the walls, backscatter is highly intermittent and, interestingly, a large backscatter follows a large forward scatter. The backscatter in the new model is an integral part of the model and not modeled separately as in stochastic backscatter models. Backscatter is approximately 50% of the net SGS dissipation and 40% of the volume exhibits backscatter.

In the previous discussion of the dynamic model (DSMAG1), the box filter with $\widetilde{\overline{\Delta}} = 2h$ was used in the homogeneous directions. Piomelli used a Fourier cutoff test filter in which the energy in the upper half of the wavenumbers in the homogeneous directions was set to zero. The ratio of length scales (test/grid) $\widetilde{\overline{\Delta}}/\overline{\Delta}$ was 2, which was found optimal by Germano *et al.* (1991). However, there was no explicit use of test filter length scale $\widetilde{\overline{\Delta}}$. If the grid filter in LES is a box filter then $\overline{\Delta} = h$, and the optimal ratio implies $\widetilde{\overline{\Delta}} = 2h$. On the other hand, the grid cannot resolve wavelength smaller than $2h$, so the filter width ought to be $\overline{\Delta} = 2h$, thus $\widetilde{\overline{\Delta}} = 4h$. To address these issues, three filters were considered, including a five point filter in the homogeneous directions with $\widetilde{\overline{\Delta}} = 4h$, a filter with $\widetilde{\overline{\Delta}} = 2h$ in all directions (volume filter), and a Fourier filter in the homogeneous directions. The differences in the

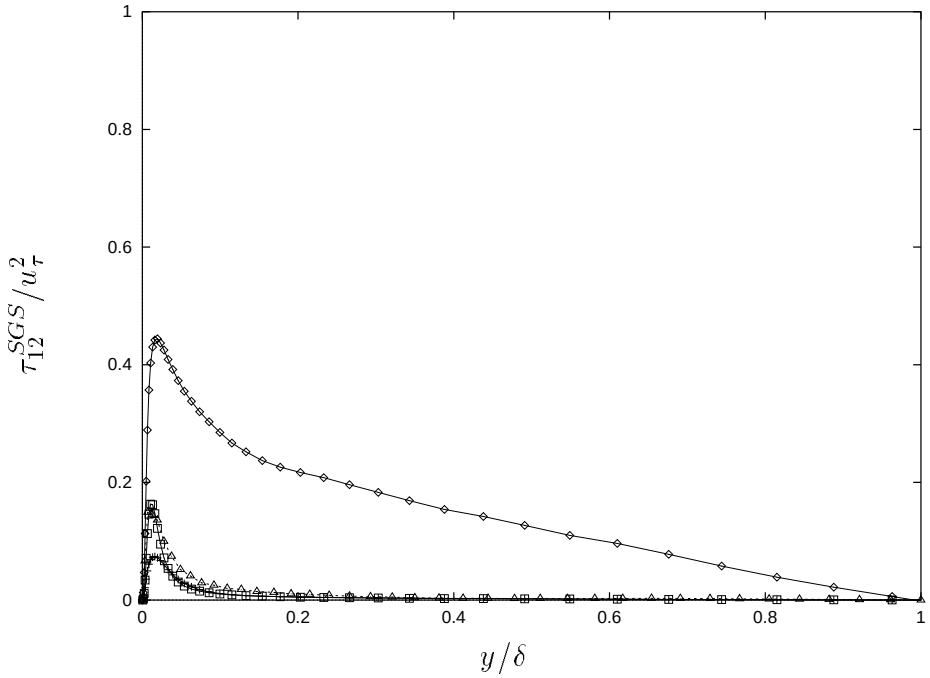

FIGURE 10. SGS shear stress at $Re_b = 38000$. —□— Smagorinsky (SMAG1); – + – dynamic (DSMAG1); —◇— proposed model (NEWM3); △ spectral LES of Piomelli (1993).

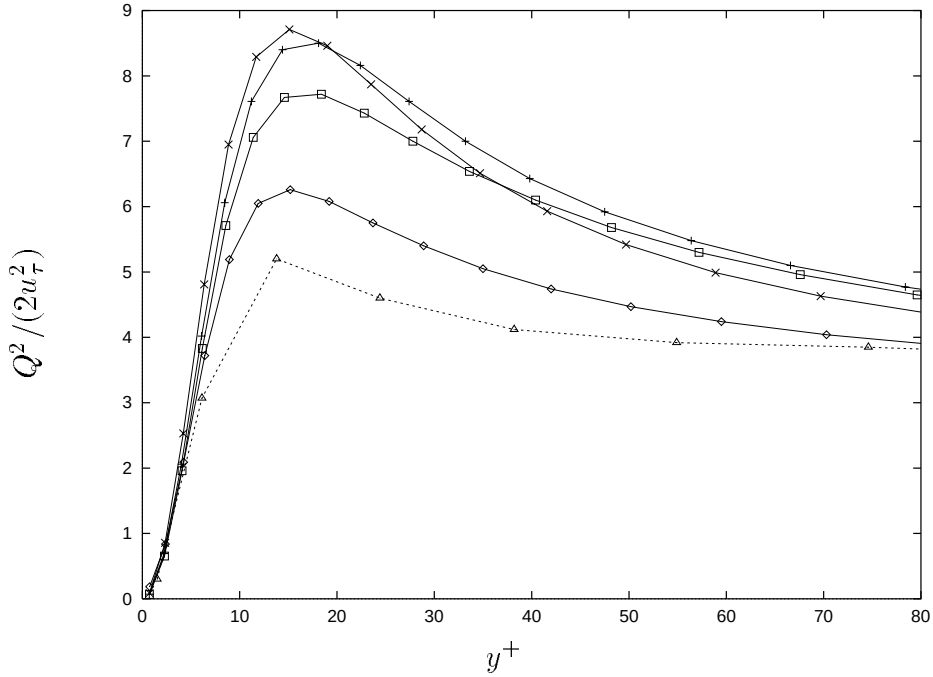

FIGURE 11. Total (resolved+SGS) turbulent kinetic energy (TKE) at $Re_b = 38000$ in wall units. Bardina's (1983) procedure has been used to estimate SGS contribution in the Smagorinsky and the dynamic model. —□— Smagorinsky (SMAG1); – + – dynamic (DSMAG1); —×— no model (CDNS1); —◇— proposed model (NEWM3); △ *resolved* TKE of Piomelli's spectral LES (1993).

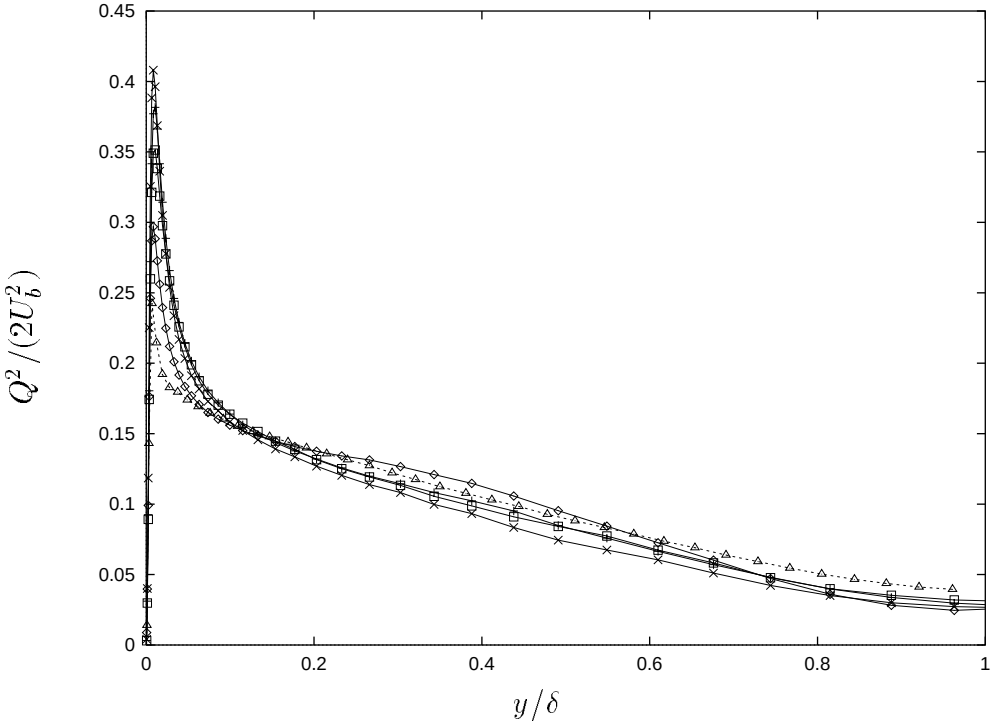

FIGURE 12. Total (resolved+SGS) turbulent kinetic energy (TKE) at $Re_b = 38000$ in global units. Bardina's (1983) procedure has been used to estimate SGS contribution in the Smagorinsky and the dynamic model. —□— Smagorinsky (SMAG1); – + – dynamic (DSMAG1); —×— no model (CDNS1); —◇— proposed model (NEWM3); △ *resolved* TKE of Piomelli's spectral LES (1993).

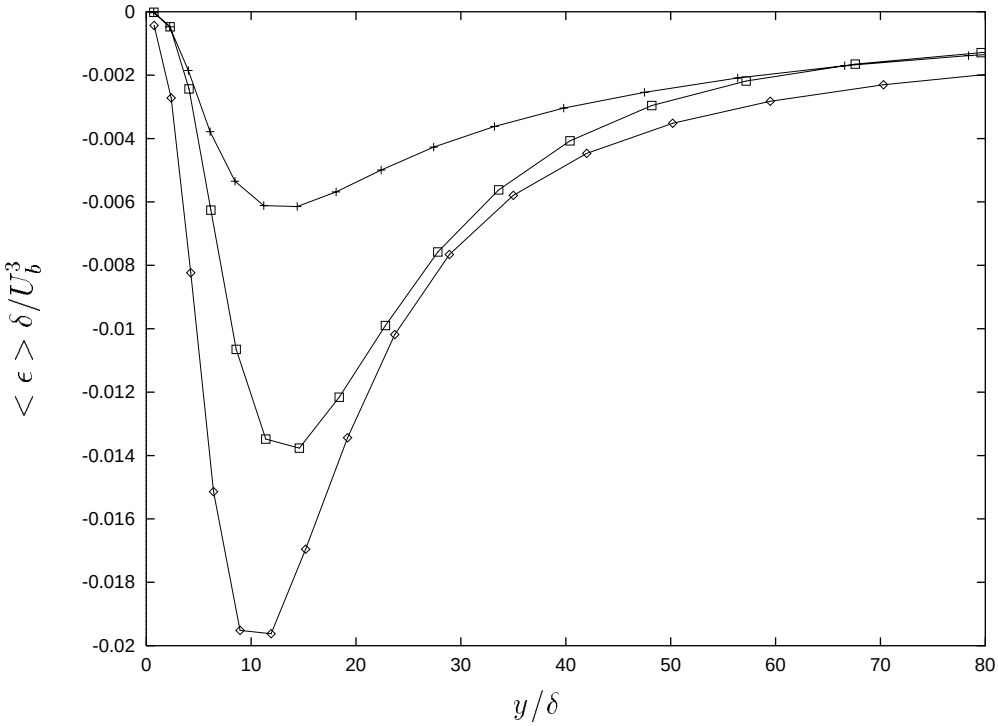

FIGURE 13. SGS dissipation rate at $Re_b = 38000$ in global units. —□— Smagorinsky (SMAG1); – + – dynamic (DSMAG1); —◇— proposed model (NEWM3).

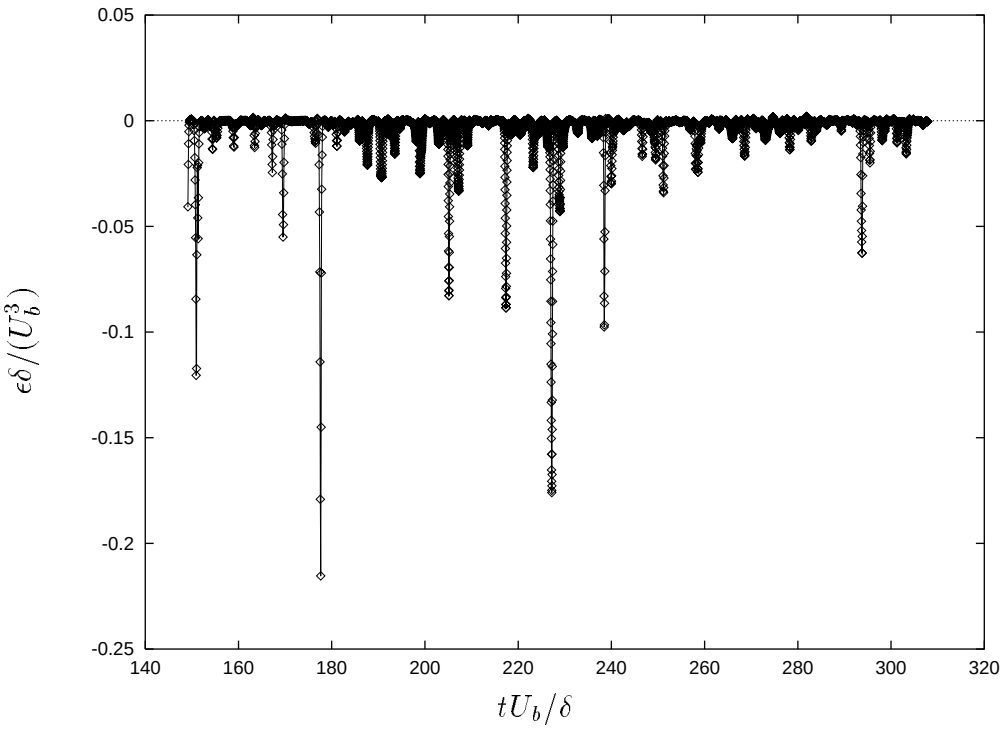

FIGURE 14. Time series of SGS dissipation rate at $Re_b = 38000$ for the proposed model (NEWM3) at $x = 1.25\pi, z = 0.25\pi$ and $y^+ = 2.3$. Positive values signify backscatter.

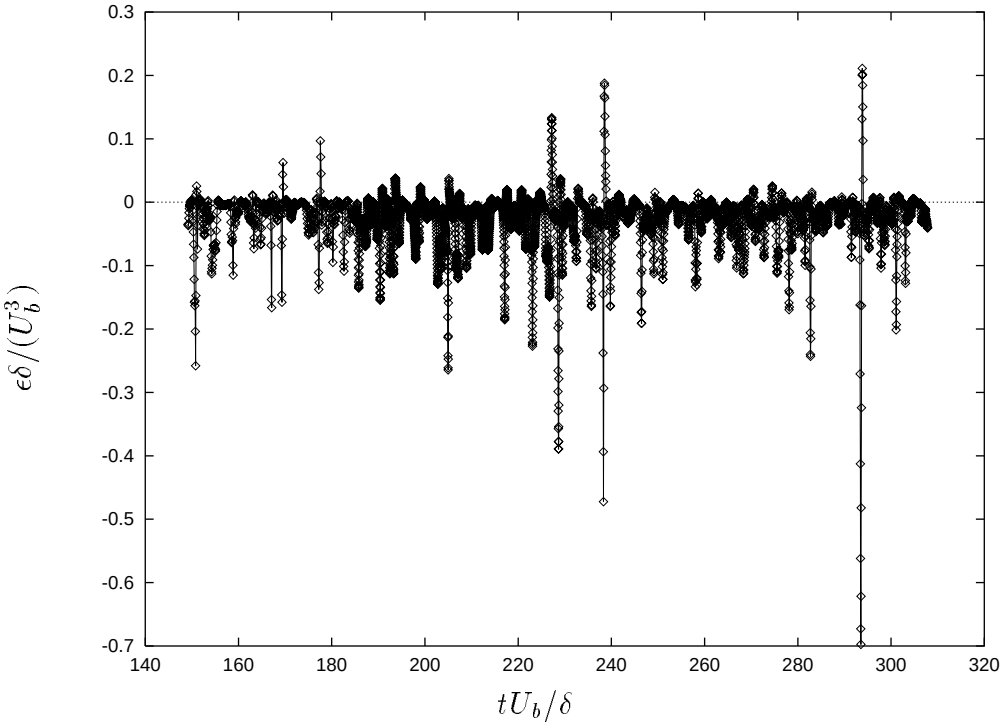

FIGURE 15. Time series of SGS dissipation rate at $Re_b = 38000$ for the proposed model (NEWM3) at $x = 1.25\pi, z = 0.25\pi$ and $y^+ = 12.0$. Positive values signify backscatter.

mean velocity profile and fluctuations were negligible. This apparent insensitivity of the dynamic model to the type of test filter suggests that most of the contribution to the dynamic coefficient C_s comes from wavenumbers in the vicinity of the grid cutoff.

The only parameter in the proposed model is the filter-grid ratio. $FGR = 0$ gives coarse DNS. If three neighboring points in each direction are employed to construct the filter, the maximum filter width is $2h$. In the current simulations same filter-grid ratio was used in defining the * and $\widehat{\ }$ operations. The dissipation is reduced considerably if the filter-grid ratio in the definitions of the * and $\widehat{\ }$ operations do not match. As shown earlier, if * corresponds to $FGR = 0$ and $\widehat{\ }$ corresponds to the grid filter, then Bardina's scale similarity model is recovered. For homogeneous turbulence the optimal FGR should be ≈ 1.0 if a box filter is used. For general inhomogeneous flows there is no clear optimal FGR, although it depends on the mesh size h. As mentioned earlier, the coefficients need not be based on the FGR, and the filter width can have directional dependence. In the present cases, the filter-grid ratio is taken to be a constant and same in all three directions. Three simulations were carried out using $FGR = 1.0$, $\sqrt{3}$, and 2.0. Increasing FGR corresponds to a larger filter width so the subgrid scales are more energetic. The mean velocity and skin friction are insensitive to variation in FGR. The effect of FGR is more pronounced in SGS stress and dissipation rate near the wall. As expected, an increase in FGR leads to larger SGS stresses and dissipation, thus smaller fluctuations in the filtered field. As far as total fluctuations are considered, $FGR = 2.0$ gives the best results. Figure 16 presents a plot of the fraction of turbulent kinetic energy in SGS versus FGR; the fraction of TKE in the SGS increases as $FGR^{0.3}$. For high Reynolds number homogeneous isotropic turbulence with a Kolmogorov energy spectrum, it is possible to estimate the turbulent kinetic energy in the subgrid scales.

$$TKE^{SGS} = \int_k^\infty E(k)\, dk \sim \epsilon^{2/3}\ k^{-2/3} \sim \epsilon^{2/3}\ \Delta^{2/3}$$

where the Kolmogorov spectrum $E(k) \sim \epsilon^{2/3}\ k^{-5/3}$ was used. The 2/3 slope is not obtained in the present LES; the subgrid-scales in the new model are highly anisotropic and the Reynolds number is too low.

3. Conclusion and future plan

A new non-eddy viscosity model has been presented in which the SGS stress is constructed by exciting the high wavenumbers of the filtered field. Its utility was demonstrated for plane channel flow with second order finite differences. The model provides a good representation of the SGS dissipation and predicts total stresses more accurately, especially at high Reynolds numbers in which a significant portion of the energy resides in the unresolved scales. The skin friction and centerline velocity are predicted accurately. The Smagorinsky and dynamic models produce lower net dissipation than the new model, leading to under-prediction of skin friction. At the mid-channel, all models produce similar fluctuations. Overall, the dynamic

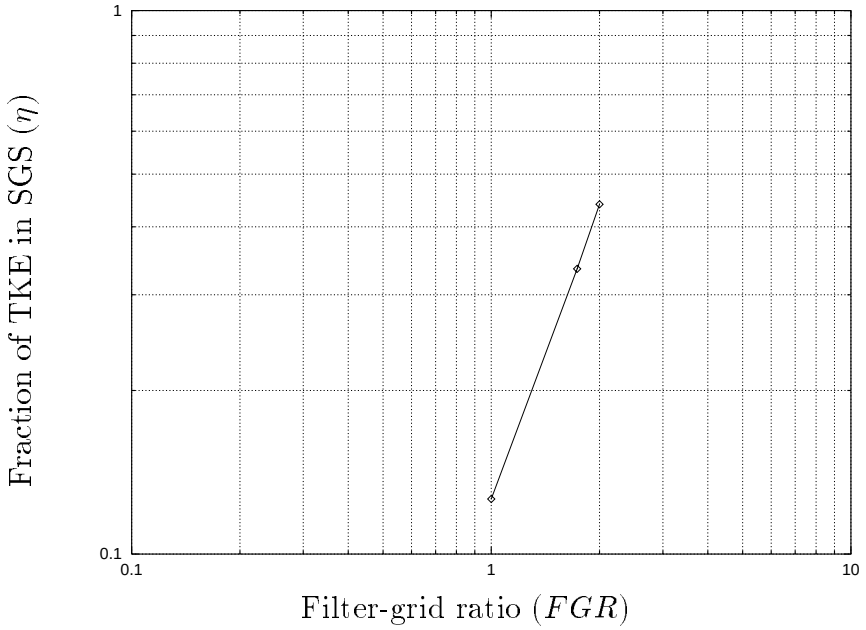

FIGURE 16. Fraction of turbulent kinetic energy in the subgrid-scales for various values of filter-grid ratio (FGR) in the proposed model.

model gives the worst results and is insensitive to the test filter. Piomelli (1993) obtained good results with a similar dynamic model but with a spectral method, so the present results suggest that the second order central differences contaminate the high wavenumber information used by the dynamic procedure. Fluctuations spectra were examined for aliasing errors but the effects were small.

A constant filter-grid ratio was used in the proposed model; however, more tests should be performed to study the effect of this parameter. Also, since backscatter is a prominent feature of this model, it should be tested in situations where backscatter is important such as transitional and geophysical flows. It could also be applied to the plane asymmetric diffuser problem for which other models under-predict separation (Kaltenbach 1994).

Finite difference simulations with better resolution need to be performed to investigate the effect of truncation errors. Also since the dynamic model seems to be sensitive to high wavenumber content, finite difference schemes with better spectral accuracy may be more successful.

The new model is efficient and easy to implement. In the present implementation, the new model takes 7% more CPU time than coarse DNS (same as Smagorinsky), whereas the dynamic model takes 30% more CPU time than coarse grid DNS, on a CRAY C90.

4. Acknowledgments

We are grateful to Dr. Tom Lund for stimulating discussions and thoughtful advice. Computing resources were provided by the San Diego Supercomputer Center (SDSC).

REFERENCES

BARDINA, J. 1983 Improved turbulence models based on large eddy simulation of homogeneous, incompressible, turbulent flows, *Ph. D. dissertation*, Dept. Mech. Engr., Stanford University, Stanford, California, USA.

CABOT, W. 1994 Local dynamic subgrid-scale models in channel flow. *Annual Research Briefs - 1994.* Center for Turbulence Research, NASA Ames/Stanford Univ. 43-159.

DEAN, R. B. 1978 Reynolds number dependence of skin friction and other bulk flow variables in two-dimensional rectangular duct flow. *J. Fluids Eng.* **100,** 215-223.

GERMANO, M. 1986 A proposal for a redefinition of the turbulent stresses in the filtered Navier-Stokes equations. *Phys. Fluids.* **29** (7), 2323-2324.

GERMANO, M., PIOMELLI, U., MOIN, P., & CABOT, W. H. 1991 A dynamic subgrid-scale eddy viscosity model. *Phys. Fluids.* **A 3** (7), 1760-1765.

GHOSAL, S., LUND, T. S., MOIN, P., & AKSELVOLL, K. 1995 A dynamic localization model for large-eddy simulation of turbulent flows. *J. Fluid Mech.* **286,** 229-255.

HÄRTEL, C.& KLEISER, L. 1993 Energy Transfer between large and small scales in wall-bounded turbulent flows. *Engineering Applications of Large Eddy Simulations FED ASME.* **162,** 21-28.

KALTENBACH, H.-J. 1994 Large-eddy simulation of flow through a plane, asymmetric diffuser. *Annual Research Briefs - 1994.* Center for Turbulence Research, NASA Ames/Stanford Univ. 175-184.

KIM, J., MOIN, P., & MOSER, R. 1987 Turbulence statistics in fully developed channel flow at low Reynolds number. *J. Fluid Mech.* **177,** 133-166.

LILLY, D. K. 1992 A proposed modification of Germano subgrid-scale closure method. *Phys. Fluids.* **A 4 (3),** 633-635.

LUND, T. S., GHOSAL, S., & MOIN, P. 1993 Numerical experiments with highly-variable eddy viscosity models. *Engineering Applications of Large Eddy Simulations FED ASME.* **162,** 7-11.

PIOMELLI, U. 1993 High Reynolds number calculations using the dynamic subgrid-scale stress model. *Phys. Fluids.* **A 5**(6), 1484-1490.

SHAH, K. 1996 Large eddy simulation of flow past a cubic obstacle, *Ph. D. dissertation*, under preparation, Dept. Mech. Engr., Stanford University, Stanford, California, USA.

VAN DRIEST E. R. 1956 On the turbulent flow near a wall. *J. Aerospace Sci.* **23,** 1007-1011.

YANG, K.-S., & FERZIGER, J. H. 1993 Large eddy simulation of turbulent flow in a channel with a surface-mounted two-dimensional obstacle using a dynamic subgrid-scale model. *AIAA Journal.* **31,** 1-8.